Soft Matter

PAPER

View Article Online
View Journal | View Issue

Cite this: *Soft Matter*, 2026, **22**, 1591

One-pot polymer–clay composite reversible adhesive

Adriana Sierra-Romero, * Emmanuel Abotsi, Katarina Novakovic and Mark Geoghegan

Received 13th October 2025,
Accepted 23rd January 2026

DOI: 10.1039/d5sm01039j

rsc.li/soft-matter-journal

Polymer–clay composites are produced using emulsion polymerization to create water-based formulations that exhibit reversible adhesion, which is triggered by alkaline or acidic aqueous solutions. These adhesives produce lap shear strengths greater than 1 MPa on a variety of substrates. A polyanionic composite is prepared by incorporating negatively charged montmorillonite into an emulsion of styrene and butyl acrylate with poly(acrylic acid) grafted from the particles. An analogue polycationic composite is made by integrating positively charged hydrotalcite into an emulsion stabilized by the physisorption of chitosan. When two substrates are both coated with the polycationic composite, reversibility is observed under acidic conditions, whereas polyanionic composites exhibit similar behaviour under alkaline conditions. Notably, polyanionic composites fully detach from the substrates, eliminating the need for additional washing. Clays also enhance the rheological behaviour of the emulsions, increasing the viscosity at low shear rates by up to 8 and 800 times, for polyanionic and polycationic formulations, respectively. These composite adhesives are a key development for facilitating the dismantling of products and enhancing recycling efficiency.

Introduction

When considering the use of adhesives within zero-waste systems, their reversibility becomes relevant as it will determine the fate of waste products. The development of reversible adhesives (often described as debond-on-demand) has targeted physical or chemical changes in their environment to trigger debonding. The most relevant involve a change in temperature, humidity, electrical potential, radiation, magnetism, or pH.[1–3] While these approaches have been successful in creating new adhesive technologies, their use can be hindered by a number of factors including complex synthetic methodologies, and substrate and application incompatibility.[3–5]

Adhesive systems that are reversible by a change in pH have been demonstrated to have significant potential. These systems rely on the presence of polyelectrolytes with opposite charges that interact to create electrostatic adhesion.[6] As polycations and polyanions lose their charges under either alkaline or acidic aqueous conditions, such adhesive bonds fail.

Recently, a method has been developed to enable the incorporation of a pH-reversible adhesive into industrial processes where the recycling or dismantling of the elements they join is important. A pair of polymer emulsion formulations containing chitosan as polycation and poly(acrylic acid) as polyanion has been reported to work in this way.[7] Here, the polyelectrolytes acted as shells to a poly(styrene-*co*-butyl acrylate) core synthesized by emulsion polymerization. One substrate was coated with the anionic formulation and the other with the cationic one allowing electrostatic adhesion with permanent failure obtained by immersion in an alkaline or acidic aqueous media. However, widespread applicability of this adhesive couple in industrial scenarios is hindered by their low viscosity, the need for a pair of emulsions instead of a single formulation, and the relatively long time taken to detach the adhered substrates.

Clays have promise as additives for such reversible adhesive systems for four reasons: first, they have been extensively used as thickening agents for economic and environmental purposes.[8] Second, they function as mechanically reinforcing fillers for a variety of polymeric materials.[9] Third, the charged nature of some species makes them attractive within the context of electrostatic adhesion.[10] Finally, they are readily available, inexpensive, and well understood.

Bentonite, which mostly consists of montmorillonite (MMT), is a smectite clay characterized by its water absorption capabilities. Its structure consists of two tetrahedral Si^{4+} sheets separated by an octahedral Al^{3+} sheet, both of which contain substitutions with lower valence cations, *e.g.*, Al^{3+} instead of Si^{4+} and Fe^{2+} or Mg^{2+} instead of Al^{3+}.[11] This imbalance produces negative charges that attract cations and contributes to their cation exchange capacity. It has been reported that MMT has a zeta

School of Engineering, Newcastle University, Newcastle Upon Tyne, NE1 7RU, UK.
E-mail: adriana.sierra-romero@newcastle.ac.uk

potential of around −30 mV with slightly higher values in acidic environments and lower in alkaline conditions.[12,13]

Layered double hydroxides are clays that consist of brucite-like sheets where bivalent ions are sometimes substituted by trivalent ions, producing positive charges that attract anions.[14] Hydrotalcite (HTC) is a commercially available example of such a clay, in which Mg^{2+} is substituted by Al^{3+}.[15] Reports on zeta potential vary greatly among sources. However, they all agree that its zeta potential is positive, increases as pH decreases, and decreases in alkaline conditions.[16,17]

The use of clays in adhesive formulations for mechanical reinforcement has been widely investigated. For instance, montmorillonite has been incorporated into waterborne latexes to improve their shear adhesion failure temperature, shear resistance, and energy of adhesion.[18] It has also been used to improve the adhesive properties of pressure-sensitive adhesives and new bio-based adhesives.[19,20] Hydrotalcite, in comparison, has mostly been used as fillers to produce coatings, polymer composites for general applications and biomedical adhesives.[21–24] However, their effect on pH-switchable polymer emulsion systems has not yet been established.

Here, we describe how the incorporation of clay into polyelectrolyte-shelled polymer nanoparticle formulations synthesized by emulsion polymerization improves both adhesive strength and reversibility. As HTC is positively charged, it was used in the preparation of polycationic emulsion composites. MMT, being negatively charged, was used in the polyanionic formulations. The formulations were characterized using particle size analysis, which was conducted to assess stability and clay dispersion within the emulsions; rheology, which was used to investigate the role of clays as potential viscosity modifiers; and transparency, which allowed an assessment of clay dispersion and exfoliation, and a consideration of visual aesthetics. Lap shear tests were carried out on various substrates to determine how clay content affects adhesive strength. Finally, the reversibility of both paired adhesive systems and individual formulations was evaluated under acidic, neutral, and alkaline conditions.

Experimental

Materials

Sodium dodecyl sulfate (SDS) ($NaC_{12}H_{25}SO_4$, ≥98.5%), chitosan (Chi) (medium molecular weight, 75% deacetylation), acetic acid (AAc) (CH_3COOH, 99.8–100.5%), styrene (St) (C_8H_8, ≥99%), butyl acrylate (BA) ($C_7H_{12}O_2$, stabilized for synthesis), acrylic acid (AA) ($CH_2CHCOOH$, 99%), potassium persulfate (KPS) ($K_2S_2O_8$, ≥99.0%), Pluronic® F-127 ($(C_3H_6O{\cdot}C_2H_4O)_x$), polysorbate 80, and synthetic hydrotalcite from Sigma-Aldrich, and sodium bentonite from Alfa Aesar were used as received for the synthesis of the composite emulsions. Hydrochloric acid (HCl) (37%), and sodium hydroxide (NaOH) (≥98%) from Sigma-Aldrich were used as received for reversibility, swelling, and contact angle tests. Mylar® plastic films (PET) 0.25 mm thick and polypropylene (PP) plastic films 0.127 mm thick were purchased from RS Components and used for the reversibility experiments. Mylar® plastic films (PET) 0.25 mm thick, polypropylene plastic films 0.45 mm thick, aluminium 1050A sheets 1.2 mm thick, polycarbonate plates 1 mm thick and Gorilla PVA glue were purchased from RS Components and used for the lap shear strength measurements. The PVA glue provides a real-world comparison for the adhesive quality of the formulations described herein.

Synthesis of poly(styrene-*co*-butyl acrylate)/poly(acrylic acid)–montmorillonite emulsion composites

A dispersion of 17.5 mg mL^{-1} of MMT in deionized water was prepared by magnetically stirring for 24 h, followed by 3 h of sonication in an Ultrawave QS12 ultrasonic bath operating at 200 W and a frequency of ∼35 kHz. This was left to settle for 24 h and the supernatant separated for future use. The clay precipitate was dried, weighed and the MMT content in suspension calculated. To prepare the emulsion, a dispersion of 20 mL deionized water containing purified clay at different concentrations (0, 0.25, 0.50, 0.75, 1.0, 1.25, and 1.5 wt%, which are samples A0 to A150) was stirred for an hour before the emulsion polymerization was performed at 70 °C as previously reported using 8.1 g of monomers at 2 : 3 St : BA mass ratio, at 450 rpm for the first 2 h and 550 rpm after the addition of AA, where initiator was added before heating and after 2 h.[7] These samples are referred as P(St–BA)/PAA–MMT.

Synthesis of poly(styrene-*co*-butyl acrylate)/chitosan–hydrotalcite emulsion composites

A dispersion of HTC at different concentrations (0, 0.25, 0.50, and 0.75 wt%, samples C0 to C75) in a Chi solution was prepared by adding the HTC to 20 mL of deionized water containing 1.0 wt% AA and 0.2 g of Chi. This was stirred for 24 h at 35 °C and 500 rpm, followed by 3 h of sonication in an Ultrawave QS12 ultrasonic bath operating at 200 W and a frequency of ∼35 kHz. Afterwards, 0.1 g of Chi was added and the dispersion stirred at 500 rpm for a further 2 h. The emulsion polymerization was carried out at 70 °C as previously reported using 8.1 g of monomers at 2 : 3 St : BA mass ratio at 550 rpm, where initiator was added before heating.[7] These samples are referred as P(St–BA)/Chi–HTC.

Synthesis of poly(styrene-*co*-butyl acrylate)/chitosan–hydrotalcite/polysorbate 80 emulsion composites

To improve the stability of HTC composite formulations, a surfactant, polysorbate 80 (PS80) was added. A 20-mL dispersion of HTC at different concentrations (0.25, 0.50, 0.75 wt%, samples CPS25, CPS50, and CPS75, respectively) was prepared in a PS80 solution 1 : 2 HTC : PS80 mass ratio. This was stirred for 24 h at 350 rpm, followed by 3 h sonication in an Ultrawave QS12 ultrasonic bath operating at 200 W and a frequency of ∼35 kHz. Emulsion polymerization was then performed at 70 °C as reported previously using 8.1 g of monomers at 2 : 3 St : BA mass ratio at 550 rpm, where initiator was added before heating.[7] These samples are referred as P(St–BA)/Chi–HTC/PS80.

Lap shear tests

Lap shear tests were performed with as-purchased substrates joined by the adhesives using a Shimadzu tester fitted with a 1 kN load cell at a speed of 1 mm min^{-1}. The substrates consisted of Mylar (biaxially oriented polyethylene terephthalate or PET), polypropylene (PP), aluminium (Al), and polycarbonate (PC) films previously cleaned with isopropanol. The lap area was set to 25.4 mm by 12.7 mm (following the ASTM D1002 standard), and tests were done in quintuplicate with the mean shear strength reported. Samples were prepared by spreading 0.05 mL of the adhesive formulation with a pipette tip as roller on both substrates, which were then pressed into contact and left to dry in a fume cupboard. For the dual adhesive system, the same protocol was followed but using the chosen complementary formulations based on the best performing sample on each substrate. On PET and PP the relevant formulations are: A0–C0 (*i.e.*, A0 on one substrate and C0 on the other), A100–C75, and A100–CPS25; on Al, A0–C0, A125–C50, and A125–CPS75; on PC, A0–C0, A75–C25, and A75–CPS50.

Viscosity

The viscosity at steady shear conditions of the emulsions at 25 °C was evaluated using an Anton Paar Modular Compact Rheometer 302e fitted with a PP50 (50 mm) parallel measuring plate at shear rates between 0.1 s^{-1} and 1000 s^{-1}. The gap between plates was 1 mm and approximately 2 mL of sample were used for testing. Measurements were performed on single representative formulations.

Swelling capability tests

The swelling of emulsion composite films was evaluated by an immersion assay at room temperature (20 °C) under static conditions. Samples were prepared by casting films on 1 cm^2 silicon moulds. Briefly, a volume of ~0.3 mL of emulsion was poured on the mould and left to dry completely. Tests were performed in triplicate by immersing dry samples (W_0) in deionized water, HCl solution at pH 1, or NaOH solution at pH 14. After 48 h, the films were wiped to remove excess liquid, weighed (W_1), and the equilibrium swelling percentage (ES%) calculated using

$$ES\% = 100 \times \frac{W_1 - W_0}{W_0}. \quad (1)$$

Reversibility of adhesion

The reversibility of adhesion was evaluated at pH 1, 7, and 14 HCl or NaOH solutions under static conditions. Debonding solutions were prepared from 1 M NaOH or HCl solutions where pH was determined using a Fisherbrand FE150 benchtop pH meter. Samples were prepared by coating PET and PP 1 cm^2 (1 cm × 1 cm) films with each emulsion composite and left to dry at room temperature (20 °C) for at least 24 h. Samples (in triplicate) were immersed in each solution and their condition evaluated periodically. Table 2 identifies each sample.

The reversibility of sample A100 was tested under the following conditions. One hundred samples (flakes) were prepared by coating PET and PP 1 cm^2 (1 cm × 1 cm) films with the A100 emulsion composite formulation. The samples were washed at a 1 : 4 mass ratio of flakes to solution (NaOH 1.0 wt%, 0.3 wt% Pluronic F127) at 85 °C and 500 rpm (overhead stirrer with a shaft of rectangular paddles). The adhesion was periodically monitored and the time it took for all samples to fail, recorded. A control experiment was set using the dual A0–C0 system (A0 on PET and C0 on PP, and A0 on PP and C0 on PET), and the adhesion monitored for the same time as in the previous test. This procedure was adapted from the "Recyclability evaluation protocol for labels and adhesives on PET bottles" published by RecyClass.[25]

Particle size measurements

The particle size distribution was measured by means of laser diffraction using a Malvern Panalytical Mastersizer 3000+ Lab. Laser obscuration was ~4.0 for clay and A0, A1, and A6 samples, and ~2.0 for C0, C25, C75, CPS25, and CPS75 samples at a stirring speed of 2500 rpm.

Contact angle

Static contact angles were measured by setting a 10 μL droplet of water pH 7, HCl solution pH 1 or NaOH solution pH 14 on an emulsion composite film and pH 7 for the different substrates. The contact angle was measured using an Ossila goniometer and associated software. Data were only recorded for droplets that retained a circular profile from above. Composite films were cast on microscope slides and dried in a fume cupboard at ambient conditions.

Scanning electron microscopy

Scanning electron micrographs for representative film samples were obtained using a Jeol JSM-IT510 microscope at a voltage of 10.0 kV and a working distance of 10.0 mm at different magnifications. Films were cast on sample holders, dried in a fume cupboard at ambient conditions and coated with gold for analysis.

UV-VIS spectrometry

The absorbance of films at 550 nm was measured using a BMG LABTECH, FLUOstar Omega Microplate Reader UV-VIS spectrophotometer. Samples were prepared in a well plate by pouring 0.2 mL of each emulsion in each 14.5 mm-diameter well and drying them at room temperature. Transmittance was calculated using

$$\%T = 10^{(2\ -\ A)}, \quad (2)$$

where A is the absorbance at 550 nm, as recommended by the ASTM method D1746-92.[26]

Attenuated total reflection infrared spectroscopy (ATR-FTIR)

ATR-FTIR spectra of PET and PP films were acquired using an Agilent Cary 630 instrument. Spectra were obtained before adhesion from sample A100, with adhesive residue and at five random locations after debonding from 650 cm^{-1} to 4000 cm^{-1}

taking 64 scans per spectrum, with a resolution of 4 cm^{-1}. For debonding, the joint was exposed to NaOH solution at pH 14 until detachment occurred. Control films with adhesive residue were obtained by mechanically breaking the joint.

Results and discussion

Physical properties of polymer–clay emulsion composites

The emulsion polymerization of a hydrophobic core of styrene (St) and butyl acrylate (BA) with a polyelectrolyte shell of either chitosan (Chi) or poly(acrylic acid) (PAA) was performed *in situ* in clay dispersions. Anionic emulsion composites were prepared in a purified bentonite (MMT) dispersion in water, while cationic formulations, in a hydrotalcite (HTC) dispersion in either Chi or polysorbate 80 (PS80) solutions. Anionic emulsions are identified as P(St–BA)/PAA or P(St–BA)/PAA–MMT while cationic formulations as P(St–BA)/Chi, P(St–BA)/Chi–HTC or P(St–BA)/Chi–HTC/PS80. A scheme illustrating them is shown in Fig. 1. To simplify identification when comparing clay content, samples are labelled as follows: A0–A150 for anionic formulations containing 0 to 1.5 wt% of MMT (in increments of 0.25 wt%, so that A25 refers to the formulation with 0.25 wt% MMT) in the initial dispersion; C0–C75 for cationic formulations containing 0 to 0.75 wt% of HTC; and CPS25–CPS75 for cationic formulations with 0.25, 0.50, and 0.75 wt% of HTC, prepared using a 2 : 1 weight ratio of PS80 to HTC.

Monomer conversion percentages and solid mass fractions were determined gravimetrically upon completion of the polymerization reaction and are presented in Table S1. Sample A0 has a solid mass fraction of 29.3 ± 0.7% and a monomer conversion of 98.4 ± 2.3%. Solid mass fraction for polyanionic composites vary between 29.2% and 29.4% while their monomer contents range from 97.7% to 98.2%. These values do not follow a defined trend, and the difference is trivial suggesting that the presence of MMT clay does not significantly affect polymerization kinetics. Sample C0 possesses a solid mass fraction and monomer conversion of 22.6 ± 0.8% and 78.9 ± 2.8%, respectively. For polycationic composites, the solid mass fractions range from 23.1% to 24.1% and the monomer conversion from 80.0% to 82.6%. In this case, the slight increase in these parameters when comparing pristine emulsion to composites may be related to the ionic strength of the medium, which influences the reaction kinetics.[27]

P(St–BA)/PAA–MMT emulsions were stable during the synthesis process and for testing at initial MMT contents of up to 1.5 wt%. Above such a clay concentration, emulsions form agglomerates during synthesis and cannot be studied. P(St–BA)/Chi–HTC samples were stable during synthesis and testing up to an initial HTC concentration of 0.75 wt% but destabilize as early as after three weeks when signs of agglomeration and sedimentation appear. Hence, a non-ionic surfactant PS80 was added at a 2 : 1 PS80 to HTC weight ratio prior to clay dispersion in Chi to improve stabilization.

Stability in emulsion composites depends on the agglomeration (*i.e.*, particle size increase and subsequent sedimentation) that they experience, especially at higher clay concentrations. Particle sizes, distribution as percentiles and spans for representative samples are shown in Table 1. Plots are included in Fig. S1 in the SI. For polyanionic formulations, the median particle size (d50) increases from 5.49 μm in sample A25 to 12.6 μm in A150, indicating the formation of larger particles during synthesis. These larger sizes may result from a combination of polymer particle growth, clay agglomeration, or polymer–clay aggregates. A similar trend is observed in polycationic formulations, where d50 is higher for samples C75 and CPS75 than for C25 and CPS25, respectively. The addition of PS80 demonstrates a clear stabilizing effect, as particle sizes decrease compared to samples prepared without the surfactant: sample C75 has a d50 of 34.4 μm, approximately double that of CPS75, which is 17.7 μm. The data also indicate that polycationic composites (C25–C75) generally possess larger particle

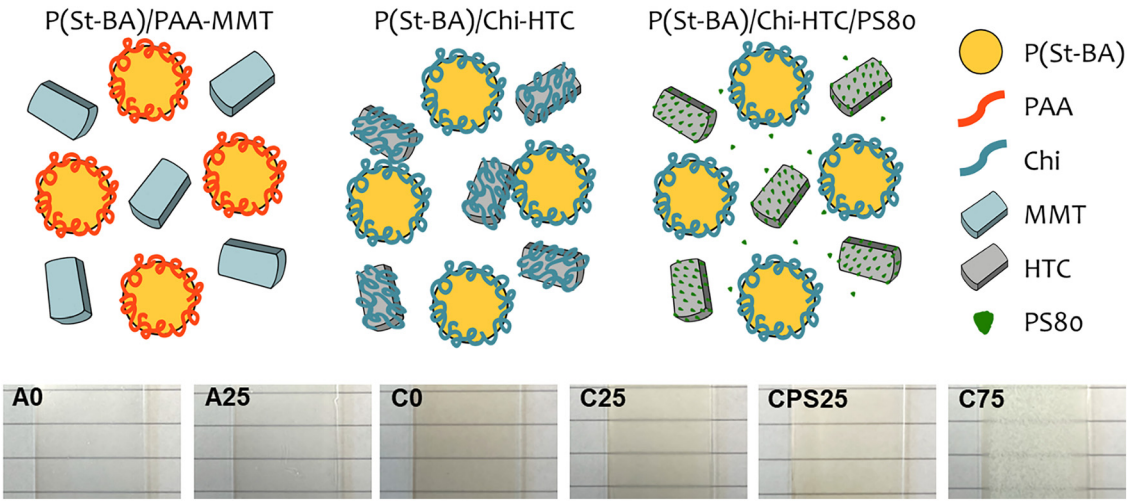

Fig. 1 Scheme illustrating the different formulations and films produced by representative composite emulsions. The backdrop is a 7 mm ruled paper.

Table 1 Representative percentiles for particle sizes and spans

Sample	d10 [μm]	d50 [μm]	d90 [μm]	Span
MMT	1.68	3.79	7.42	1.51
HTC	0.54	2.60	5.45	1.89
A0	3.03	6.35	12.4	1.47
A25	1.69	5.49	10.1	1.53
A150	5.89	12.6	23.8	1.42
C0[a]	0.0217	0.0718	0.297	3.84
C25	12.9	24.4	42.4	1.21
C75	17.3	34.4	151	1.34
CPS25[a]	0.0262	0.118	4.04	34.0
CPS75	7.6	17.7	32.6	32.6

[a] Results may be less accurate due to the instrument's limited sensitivity at lower size ranges. Results in this region should be interpreted with caution.

sizes than their polyanionic counterparts, which helps explain the narrower range of clay contents suitable for stable synthesis. For example, C25 exhibits a d50 of 24.4 μm, whereas A25 has a d50 of 5.49 μm.

The inclusion of clay platelets introduces new platelet–polymer interactions such as hydrogen bonds, and ionic or electrostatic interactions between polymers and minerals where intercalation is a possibility.[28,29] Overall, larger particle sizes render the systems unstable by promoting processes such as sedimentation, flocculation, and coalescence. In contrast, pristine emulsions, *i.e.*, those prepared in the absence of clay, have been reported to have a stable particle size for up to a year.[7]

Alterations in particle size and size distribution imply a change not only in emulsion stability, but most importantly in the rheological behaviour of these emulsion composites. Historically, clays have been used as thickening agents due to the platelet–polymer interactions they exhibit, which have been described above, but also due to platelet–platelet interactions (*e.g.*, electrostatic interactions and van der Waals forces) that have been reported elsewhere.[28] Viscosity measurements at varying shear rates are shown in Fig. S2 (SI) while Fig. 2 presents the viscosity at a low shear rate (near rest) regimes of $\sim$0.1 s^{-1} where sagging processes occur.[30–33] These are of interest for adhesives that may be applied at high production speeds on vertical substrates. Fig. S3 shows samples A0 and A100 applied to vertical PET plastic substrates.

It can be observed how the viscosity measured at near rest conditions increases overall, particularly for cationic emulsion composites, with maximum recorded values of 225.9, 34.9, and 22.4 Pa s for samples A100, C75, and CPS50, respectively. The decrease in viscosity at higher clay content is presumably produced by the increasing particle size and size distribution of the samples, which have repercussions on the polymer–clay surface area. As particle size increases, the surface-to-volume ratio decreases, effectively lowering the interfacial area available for polymer–polymer and polymer–clay interactions to occur. Further, a broader particle size distribution generally enables more efficient packing of particles, allowing particles to move more easily around each. Combined, these two effects suggest a mechanism for the observed decrease in viscosity with increasing clay content.

Most prepared emulsions display good film formation properties with varying degrees of transparency. Photographs are shown in Fig. 1 and Fig. S4. As observed, composite films preserve transparency with the addition of clays at the lowest contents. In general, crystallites, voids, or inclusions that are larger than the wavelength of visible light will scatter light, decreasing transparency. For a composite to be transparent, the refractive index of the filler must be similar to that of the polymer matrix, and platelets must be homogeneously dispersed.[34] The refractive indexes of polystyrene and poly(butyl acrylate) are reported to be 1.59, and 1.47 respectively, with intermediate values for their copolymers; 1.55 is reported for silicates, and 1.57 for brucite.[35–39]

Film transparency was assessed by measuring percent transmittance in the visible region (550 nm) using UV-vis spectrometry, as detailed in the Experimental section. Table 2 summarizes the results. It is observed that overall, the transmittance of samples decreases with the addition of clays. For anionic films, it decreases from 46.0% for A0 to 29.5% for A150. This loss is more noticeable for cationic films. Pristine P(St–BA)/Chi emulsion film has the highest transmittance at 67.1%, which is reduced to 8.6% and 12.7% for C75 and CPS75, respectively. Transmittance

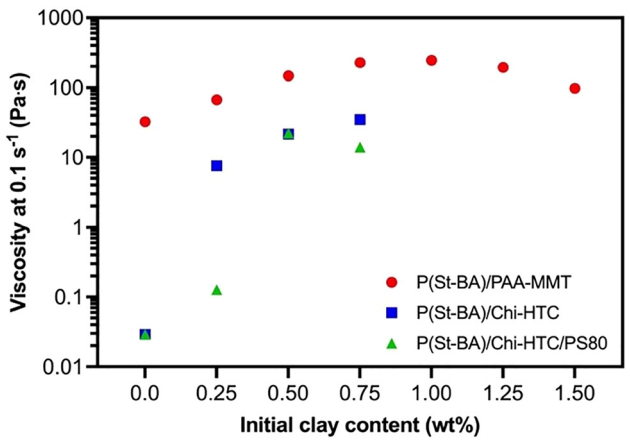

Fig. 2 Viscosity of emulsion composites at near rest (0.1 s^{-1} shear rate).

Table 2 Transparency of films

Sample	Absorbance at 550 nm	Transmittance [%]
A0	0.337	46.0
A25	0.421	37.9
A50	0.462	34.5
A75	0.446	35.8
A100	0.454	35.2
A125	0.487	32.6
A150	0.53	29.5
C0	0.173	67.1
C25	0.713	19.4
C50	0.97	10.7
C75	1.066	8.6
CPS25	0.193	64.1
CPS50	0.635	23.2
CPS75	0.896	12.7

decreases with increasing clay content due to light scattering caused by clay platelets. Higher clay contents, lead to aggregates and clusters that disrupt the uniform refractive index of the polymer matrix, leading to opacity and reduced clarity as observed in sample C75 with the presence of white sections throughout the film. The nonuniformity observed presumably arises from local phase heterogeneity or even from migration of HTC platelets to the film–air interface during drying.

To investigate the wettability of the composite emulsion films, the water contact angles for all composite films were measured and are recorded in Table S2. The cationic emulsion C0 has a water contact angle of 88.7°, which increases up to 124.4° for C75 and decreases to 65.0° for CPS75. Samples with only HTC become less wettable given the hydrophobic nature of HTC clay, which has a water contact angle of 132.8°. The opposite occurs for CPS samples due to the presence of PS80, a surfactant. The anionic emulsion A0 records a water contact angle of 30.3°, which, remarkably, is reduced to 18.5° with the inclusion of MMT in A25. It then progressively increases to 31.8° for A150. SEM images of the dry surfaces pertaining to these contact angle data are shown in Fig. S5. The effect of increasing clay content results in much more structure (roughness) in the superficial morphology of the films.

Adhesive performance of polymer–clay emulsion composites

The performance of the adhesive composites was measured through tension tests on poly(ethylene terephthalate) PET, polypropylene (PP), aluminium (Al), and polycarbonate (PC) substrates to evaluate the effect clay has on the lap shear strength of the emulsions. These results were compared to commercial poly(vinyl acetate), PVA, glue which was tested under the same conditions. Fig. 3 shows those measurements for all substrates. For P(St–BA)/PPA–MMT samples lap shear strengths of up to 1.14 ± 0.72 MPa for A100 on PET and 1.46 ± 0.15 MPa for A125 on Al were achieved, compared to 0.40 ± 0.02 MPa and 0.81 ± 0.05 MPa recorded for A0 on the same substrates. The lap shear strength of A25–A150 on PP and PC was either reduced or remained similar.

Lap shear strengths for P(St–BA)/Chi–HTC increased from 0.64 ± 0.02 MPa for C0 to 0.76 ± 0.03 for C75 on PP and from 0.71 ± 0.06 MPa to 1.42 ± 0.12 MPa for those same samples on Al. A reduction on the maximum strength was observed for PET and PC substrates. In the case of P(St–BA)/Chi–HTC/PS80 samples, a general reduction in the adhesion strength was recorded. All samples, both anionic and cationic, surpassed the lap shear strength of the PVA glue on PET (0.31 ± 0.06 MPa), PP (0.21 ± 0.02 MPa) and PC (0.38 ± 0.07 MPa), which demonstrates that the adhesives reported here are well adapted to bonding plastic surfaces, the low energy of which makes them generally difficult to adhere.

Overall, MMT and HTC act as reinforcing fillers due to their native mechanical strength given by a Young's modulus of 178–265 GPa and 140 GPa for MMT and HTC, respectively.[40,41] It has been reported that PAA can undergo physisorption and

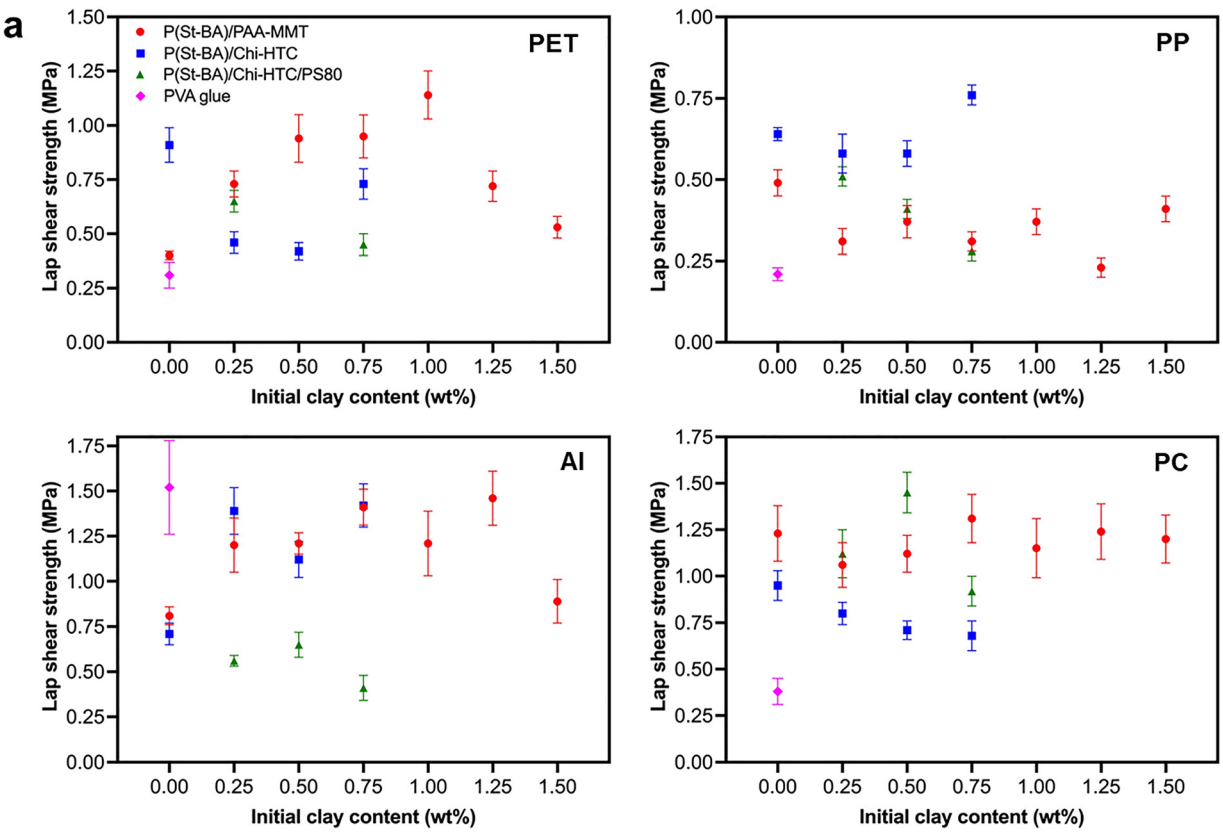

Fig. 3 Lap shear strength of composite emulsions on the substrates indicated. The legend in (a) is the same for the other images.

chemisorption processes on MMT with the formation of hydrogen bonds, of siloxane (C—O—Si) or of coordination complexes between structural cations and carboxyl groups.[42] These interactions promote an effective load transfer between the bulk of the polymer matrix and the clay platelets which act as anchor points that oppose deformation.[43] A similar behaviour is observed for HTC where Chi transfers the load to clay platelets through weak steric interactions, hydrogen bonding, and other hydrophobic interactions.[44] It has also been reported that HTC can incorporate into hydrophobic polymer matrixes, such as polystyrene.[45,46] HTC completely or partially embedded into polymer particles would correlate to the large particle sizes and contribute to the instability of the systems at higher clay contents. The presence of PS80 improves stability by lowering interfacial tension and providing steric stabilization to HTC. However, once into the dry adhesive film, PS80 behaves as a low glass transition, amphiphilic species. In general, plasticizers lower cohesive strength, reduce the modulus, and consequently decrease the maximum lap shear strength despite improving emulsion stability.[47]

Adhesion performance does not solely rely on clay acting as a filler but also on the intrinsic properties of the substrates and their compatibility with the adhesive composites. This is given by factors such as surface energy, surface roughness, and conformal contact between films, *i.e.*, interfacial geometry.[48] The substrates used in this study exhibit water contact angles of 72° (PET), 75° (Al), 86° (PC), and 87° (PP), indicating moderate to weak hydrophilicity as the contact angle approaches 90°. However, no clear correlation is observed between contact angle and adhesive strength. For example, PC and PP display similar contact angles but show markedly different adhesion performance. This suggests that surface energy alone does not govern adhesion behaviour. One possibility is that, as water evaporates, the polymer–clay component enhances hydrophobic interactions with the substrate, aided by the presence of poly(styrene-*co*-butyl acrylate), which contributes to the overall hydrophobicity of the system. Additionally, clay platelets tend to migrate toward the interface to minimize interfacial energy, leading to clay-rich regions that influence the overall morphology.[49] Substrate surface roughness plays a critical role in determining adhesion by affecting mechanical anchoring and leading to tortuous fracture paths.[48] Generally, increasing roughness enhances adhesion by providing a larger effective surface area and enabling the adhesive to penetrate micro-scale features, thereby improving mechanical interlocking. In a similar way, the presence of clays improve crack propagation resistance by pinning or deflecting fractures.[50]

Less obvious mechanisms for the observed improvement on the adhesive performance can be attributed to a complex array of interactions between polymer phases and substrate chemistries (*e.g.*, polarity, functional groups, hydrogen-bonding capability, and van der Waals interactions).[51] For instance, styrene contributes to π–π and van der Waals interactions while butyl acrylate moieties to flexibility and dispersive interactions. Polyelectrolytes introduce ionic and hydrogen bonding interaction sites. Substrates such as PET and Al possess higher polar contributions whereas PC and especially PP offer few interaction sites, making adhesion more dependent on dispersive interactions and mechanical interlocking. Thus, the measured adhesive strength arises from a combination of four factors: (1) the intrinsic surface energy of each substrate, (2) the chemical affinity of the hydrophobic segments in the adhesive, (3) the ionic functionality introduced by the polyelectrolytes, and (4) the role of clays as reinforcing agent.

Lap shear tests were also carried out for representative dual systems chosen from the highest recorded values for each adhesion couple. These results are shown in Fig. S6. The best improvement was obtained for the A100–C75 system on PET with a strength of 0.7 ± 0.05 MPa, compared to a value of 0.36 ± 0.03 MPa for A0–C0 on the same substrate. It is relevant to notice that, while the use of individual formulations leads to both adhesive and cohesive failure, the dual A–C system predominantly retains some coverage on both surfaces, which is likely to be a mix of cohesive failure and adhesive failure at the A–C interface.

Finally, it is important to note that the PET and PP substrates used in this study are considerably thinner and more compliant than Al and PC. Though no evident deformation was observed during lap shear loading, these thin substrates may undergo bending, which shifts the stress state at the adhesive joint from a predominantly shear mode to a mixed mode combination of shear and peel.[52] Such bending may influence the recorded maximum load depending on the specific deformation geometry. As a result, the lap shear strengths measured on PET and PP should be interpreted with caution, as they reflect the combined contribution of adhesive performance and substrate flexural compliance.

Reversible adhesion

The permanent reversibility of the adhesion bond was tested on PET and PP plastics, which are often used in labelling applications. Samples measuring 1 cm^2 were prepared as described in the Experimental section, and exposed to acidic, neutral, and alkaline conditions to evaluate whether the bond failed or not. The results are summarized in Table S3. It was found that the adhesive systems formed by C0–A0, C75–A100, and CPS25–A100 failed when immersed in either acidic or alkaline conditions. This behaviour is consistent with previous findings on electrostatic reversible adhesion, where the symmetry of a polycation–polyanion couple allows the pH-induced conformational transition to determine adhesive failure at both high and low pH. At low pH, the amino groups in Chi become protonated ($—NH_3^+$) while the carboxylic groups in PAA remain neutral (—COOH). At high pH, the opposite occurs: the carboxylic groups in PAA are negatively charged ($—COO^-$), and the amino groups in Chi are uncharged ($—NH_2$).[7,53] No adhesive bond failed when immersed in neutral solution.

Individual emulsion composites also display unique reversible properties. It was observed that P(St–BA)/Chi–HTC and P(St–BA)/Chi–HTC/PS80 are reversible under acidic conditions with the adhesive detaching from the PP substrate. Moreover, P(St–BA)/PAA–MMT samples not only failed when immersed in

alkaline media, but the adhesive film completely detached from the substrates as pointed out in Fig. 4.

It was previously reported that the dual adhesive system A0–C0 debonds at pH < 3 and pH > 12. It is expected that these new formulations will exhibit similar behaviour. However, this remains to be experimentally verified.

Optical microscope images of clean substrates after detachment of sample A100 are shown in Fig. S7 and FTIR-ATR spectra of clean substrates before adhesion and at five random locations after debonding are presented in Fig. S8. For PET, clean substrates and substrates after debonding show identical spectra with characteristic peaks in the fingerprint region for aromatic polyesters: 1713 cm^{-1} (C═O stretch), 1244 cm^{-1} (C—C*—O stretch, where C* is a carbonyl) and 1096 cm^{-1} (O—C—C stretch). On the PET control film, the presence of adhesive residue hinders these signals. As for PP substrates, pristine films and films after debonding produce identical spectra, while the control sample displays signals associated only to the adhesive: 1727 cm^{-1} (acrylic C═O stretch) 1452 cm^{-1} (aromatic styrene C—C stretch), and 1158 cm^{-1} (acrylic C—O stretch). These data confirm no evidence of adhesive residue on the substrate after debonding.

In the absence of clay platelets, polyelectrolytes from adjacent particles remain in direct contact, restricting chain movement and preventing the retention of maximal charge density due to Coulombic frustration. It is speculated that the platelets promote conformational rearrangements of the polyelectrolyte chains by providing spatial separation that facilitate chain mobility under appropriate pH conditions. The platelet surface charge does not appear to interfere with this process, suggesting that they act primarily as structural supports rather than as barriers to rearrangement, promoting debonding at the weaker interface (PP for P(St–BA)/Chi–HTC and P(St–BA)/Chi–HTC/PS80 composites) or at both interfaces (for P(St–BA)/PAA–MMT samples). It is also noted that the presence of clay platelets has an effect in the local ionic strength within the system that may influence chain extension at certain pH values.[54]

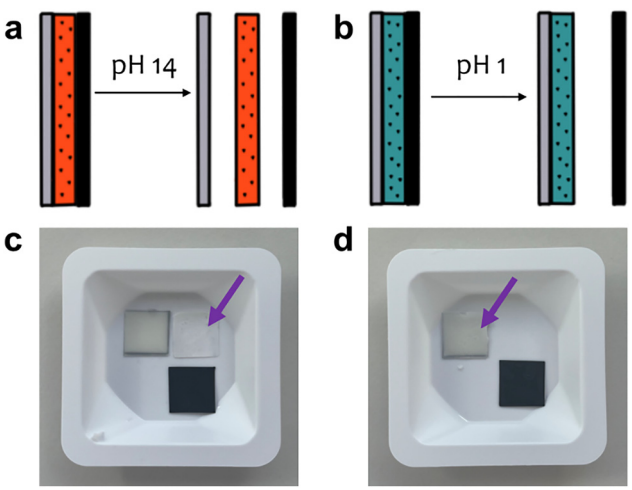

Fig. 4 Representative reversible behaviour of (a) and (c) A100 in alkaline conditions, and (b) and (d) CPS75 in acidic conditions. Arrows indicate the adhesive residue, which, for A100, had completely separated from the substrates. PET is clear and PP is black.

To evaluate reversible behaviour under a typical recyclability of plastic packaging protocol, a second test using 100 substrates bonded using A100 was performed at an elevated temperature (85 °C) and under dynamic conditions (here, stirring at 500 rpm) as described in the Experimental section. It was found that after 30 min, 42 samples had failed, after 45 min, 83 samples, and after one hour, all 100 samples had failed. Upon closer observation, it was noted that the adhesive had also detached from the substrates in all samples, which removes a potentially difficult cleaning step in recycling technologies or would allow the reuse of the substrates.

Swelling tests were performed to investigate the reason behind adhesion failure and adhesive detachment for the emulsion composites. It was first hypothesized that failure and detachment were produced by mechanical factors, where the film swelled to produce a shear stress on the substrate large enough that it leads to separation from one or both substrates. The equilibrium swelling percentages (ES%) in acidic, water, and alkaline media can be found in Fig. S9. These tests did not indicate ES% above the ones recorded for A0, so failure and detachment cannot solely be correlated to mechanical effects. Apparently, clay introduces substrate–film interactions that can be broken only at certain pH conditions. Furthermore, MMT swells in alkaline conditions,[55] so it is possible that clay plays a determining role in the failure of the film by disrupting film cohesion. This microstructural change may be potentiated at the interface where low-tack regions are formed (*i.e.*, during drying and clay migration) promoting debonding at high pH, but further investigation is required.

Furthermore, emulsion composites can also be removed using solvents such as acetone and turpentine as reported previously for the original formulations.[7] This is useful primarily for polycationic composites that remain attached to the substrate after exposure to acidic solution.

Conclusions

In summary, reversible adhesive composites can be prepared through *in situ* polymerization of polymer emulsions in clay dispersions. Polycationic emulsions were produced in the presence of HTC and HTC/PS80 dispersions polyanionic emulsions, in MMT dispersions. These formulations exhibit nearrest viscosities high enough to reduce sagging, with increases of up to 8-fold for polyanionic and up to 800-fold for polycationic composites. They display overall improved adhesive performance on PET, PP, Al, and PC substrates with lap shear strength greater than 1 MPa. Finally, the adhesion of polycationic composite formulations can be reversed under static, room-temperature acidic conditions, while polyanionic samples exhibit reversibility under equivalent alkaline environments. Remarkably, polyanionic adhesive composites are also removed from the substrate when exposed to said alkaline

media after 24 h or after 1 h when stirred at 85 °C. These formulations therefore provide a scalable, inexpensive, readily reversible water-based adhesive, that permits the disjoining of many different substrates, including difficult low-surface energy polymers. This technology is therefore a leading candidate for future recycling technologies.

Author contributions

ASR, MG, and KN conceived and designed the experiments; ASR and EA performed the experiments and analysed the data; MG and KN supervised the work; MG managed the project; ASR produced the video abstract and wrote the paper, to which all authors contributed and which all authors have approved.

Conflicts of interest

The materials described in this work are covered by two PCT patent applications (WO 2024/084210 A1 and PCT/GB2025/051976), both of which state A. S. R., K. N., and M. G. as named inventors.

Data availability

Additional results, photographs and micrographs are included in the supplementary information (SI). See DOI: https://doi.org/10.1039/d5sm01039j.

The data that support the findings of this study are available from the corresponding author upon reasonable request.

Acknowledgements

The authors acknowledge the Engineering and Physical Sciences Research Council for supporting this research through grant EP/Y008316/1. Dr Isabel Arce-Garcia and Mr Michael Wilkes are acknowledged for their help with the SEM imaging and viscosity measurements, respectively.

References

1 N. D. Blelloch, H. J. Yarbrough and K. A. Mirica, *Chem. Sci.*, 2021, **12**, 15183–15205.
2 K. R. Mulcahy, A. F. R. Kilpatrick, G. D. J. Harper, A. Walton and A. P. Abbott, *Green Chem.*, 2022, **24**, 36–61.
3 A. Sierra-Romero, K. Novakovic and M. Geoghegan, *Langmuir*, 2022, **38**, 15476–15493.
4 J. Hwang, D. Lim, G. Lee, Y. E. Kim, J. Park, M.-J. Baek, H.-S. Kim, K. Park, K. H. Ku and D. W. Lee, *Mater. Horiz.*, 2023, **10**, 2013–2023.
5 T.-H. Lee, G.-Y. Han, M.-B. Yi, H.-J. Kim, J.-H. Lee and S. Kim, *ACS Appl. Mater. Interfaces*, 2021, **13**, 43364–43373.
6 R. La Spina, M. R. Tomlinson, L. Ruiz-Pérez, A. Chiche, S. Langridge and M. Geoghegan, *Angew. Chem., Int. Ed.*, 2007, **46**, 6460–6463.
7 A. Sierra-Romero, K. Novakovic and M. Geoghegan, *Angew. Chem., Int. Ed.*, 2024, **63**, e202310750.
8 F. Karakaş, G. Pyrgiotakis, M. S. Çelik and B. M. Moudgil, *KONA Powder Part. J.*, 2011, **29**, 96–106.
9 F. Gao, *Mater. Today*, 2004, **7**, 50–55.
10 H. Cao, X. Liu, B. Feng, J. Sun, D. Ma, X. Chen and H. Li, *Sci. Rep.*, 2024, **14**, 23169.
11 P. F. Luckham and S. Rossi, *Adv. Colloid Interface Sci.*, 1999, **82**, 43–92.
12 P. García-Guzmán, L. Medina-Torres, F. Calderas, M. J. Bernad-Bernad, J. Gracia-Mora, B. Mena and O. Manero, *Colloids Surf., B*, 2018, **167**, 397–406.
13 P.-I. Au and Y.-K. Leong, *Colloids Surf., A*, 2013, **436**, 530–541.
14 D. G. Evans and X. Duan, *Chem. Commun.*, 2006, 485–496.
15 M. C. D. Mourad, M. Mokhtar, M. G. Tucker, E. R. Barney, R. I. Smith, A. O. Alyoubi, S. N. Basahel, M. S. P. Shaffer and N. T. Skipper, *J. Mater. Chem.*, 2011, **21**, 15479–15485.
16 V. P. Nguyen, K. T. T. Nguyen, L. T. Ton, D. T. Nguyen, K. Q. Nguyen, M. T. Vu and H. N. Tran, *J. Nanomater.*, 2020, **2020**, 1783749.
17 L. Fang, W. Li, H. Chen, F. Xiao, L. Huang, P. E. Holm, H. C. B. Hansen and D. Wang, *RSC Adv.*, 2015, **5**, 18866–18874.
18 A. Bonnefond, M. Mičušík, M. Paulis, J. R. Leiza, R. F. A. Teixeira and S. A. F. Bon, *Colloid Polym. Sci.*, 2013, **291**, 167–180.
19 A. K. Antosik, K. Mozelewska, Z. Czech and M. Piątek-Hnat, *Silicon*, 2020, **12**, 1887–1893.
20 G. Qi, N. Li, D. Wang and X. S. Sun, *J. Am. Oil Chem. Soc.*, 2016, **93**, 1509–1517.
21 B. M. Quy, N. T. Chinh, N. T. K. Anh, V. T. Tuyet, N. X. Thai, V. Q. Trung, N. T. C. Quyen, N. N. Tan and T. Hoang, *ChemistryOpen*, 2024, **13**, e202400120.
22 C. Xie, Y. Jia, M. Xue, Z. Yin, Y. Luo, Z. Hong and W. Liu, *Prog. Org. Coat.*, 2022, **168**, 106881.
23 N. J. M. Sebri, A. F. A. Latip, R. Adnan and M. H. Hussin, in *Green Sustainable Process for Chemical and Environmental Engineering and Science*, ed. T. Altalhi and Inamuddin, Elsevier, 2022, pp. 23–42.
24 L. Perioli, A. Dorigato, C. Pagano, M. Leoni and A. Pegoretti, *Polym. Eng. Sci.*, 2019, **59**, E112–E119.
25 RecyClass, Recyclability evaluation protocol for labels and adhesives on PET bottles, 2024.
26 J. Zhao, Y. Wang and C. Liu, *Food Anal. Methods*, 2022, **15**, 2840–2846.
27 A. S. Dunn and Z. F. M. Said, *Polymer*, 1982, **23**, 1172–1176.
28 P. F. Low, in *Advances in Fine Particles Processing: Proceedings of the International Symposium on Advances in Fine Particles Processing*, ed. J. Hanna and Y. A. Attia, Springer US, Boston, MA, 1990, pp. 209–226.
29 B. Chen and J. R. G. Evans, *J. Phys. Chem. B*, 2004, **108**, 14986–14990.
30 X. Sun, X. Lin, Y. Luo, D. Yu, W. Yan, H. Zhang, Z. Wang, C. Zhang, J. Guo, W. Zhang, W. Gao and S. Huang, *Materials*, 2024, **17**, 4626.

31 Y. Maiket, R. Yeetsorn, W. Wanchan, S. Chuayprakong, T. Ungtrakul, M. Abbas and E. Haberstroh, *Bull. Mater. Sci.*, 2024, **47**, 226.
32 J. H. Bieleman, *Chimia*, 2002, **56**, 163–169.
33 N. Crawford and F. Meyer, *Application note V291 - Investigating the shear flow and thixotropic behavior of paints and coatings*, Thermo Fisher Scientific, 2025.
34 Y. Lin, E. Bilotti, C. W. M. Bastiaansen and T. Peijs, *Polym. Eng. Sci.*, 2020, **60**, 2351–2376.
35 B. S. Mitchell, *An Introduction to Materials Engineering and Science*, John Wiley & Sons, Ltd, Hoboken, New Jersey, 2003, pp. 900–902.
36 B. Meng, J. Deng, Q. Liu, Z. Wu and W. Yang, *Eur. Polym. J.*, 2012, **48**, 127–135.
37 C. L. Lee, S. Y. Chee and M. K. Lee, *Polym. Bull.*, 2017, **74**, 857–872.
38 E. V. Vaganov, R. I. Komendant, E. O. Perepelitsina, V. P. Grachev and S. A. Kurochkin, *IOP Conf. Ser.:Mater. Sci. Eng.*, 2020, **848**, 012036.
39 R. C. Shannon, B. Lafuente, R. D. Shannon, R. T. Downs and R. X. Fischer, *Am. Mineral.*, 2017, **102**, 1906–1914.
40 B. Chen and J. R. G. Evans, *Scr. Mater.*, 2006, **54**, 1581–1585.
41 Y. Zhang and J. R. G. Evans, *Colloids Surf., A*, 2012, **408**, 71–78.
42 N. H. Tran, G. R. Dennis, A. S. Milev, G. S. K. Kannangara, M. A. Wilson and R. N. Lamb, *J. Colloid Interface Sci.*, 2005, **290**, 392–396.
43 A. Illaik, C. Taviot-Guého, J. Lavis, S. Commereuc, V. Verney and F. Leroux, *Chem. Mater.*, 2008, **20**, 4854–4860.
44 H. Kwon, J. Choi, C. Lim, J. Kim, A. Osman, Y. Jho, D. S. Hwang and D. W. Lee, *Biomacromolecules*, 2025, **26**, 1012–1022.
45 H. Benaddi, D. Benachour and Y. Grohens, *J. Polym. Eng.*, 2016, **36**, 681–693.
46 Y. Han, Y. Wu, M. Shen, T. Li, Y. Wang, Q. Zhang and Z. Wang, *Polym. Compos.*, 2017, **38**, 1680–1688.
47 K. Mishra, S. S. Pundir and D. K. Rai, *Ionics*, 2017, **23**, 105–112.
48 M. Ohring, in *Materials Science of Thin Films*, ed. M. Ohring, Academic Press, San Diego, California, 2nd edn, 2002, pp. 711–781.
49 R. Van Hooghten, S. Gyssels, S. Estravis, M. A. Rodriguez-Perez and P. Moldenaers, *Eur. Polym. J.*, 2014, **60**, 135–144.
50 M. Bashar, P. Mertiny and U. Sundararaj, *J. Nanomater.*, 2014, **2014**, 312813.
51 M. Zhao, J. Wu, F. Zeng, Z. Dong, X. Shen, Z. Hua and G. Liu, *Chem. Sci.*, 2024, **15**, 6445–6453.
52 Y. Wei, X. Jin, Q. Luo, Q. Li and G. Sun, *Composites, Part B*, 2024, **276**, 111225.
53 M. Raftari, Z. J. Zhang, S. R. Carter, G. J. Leggett and M. Geoghegan, *Macromolecules*, 2015, **48**, 6272–6279.
54 T. Jamil, J. R. Gissinger, A. Garley, N. Saikia, A. K. Upadhyay and H. Heinz, *Nanoscale*, 2019, **11**, 11183–11194.
55 S. Amiri, A. Esfandyari Bayat and S. Akbari, *Colloids Surf., A*, 2025, **707**, 135942.